

# Recognition of Dementia Biomarkers With Deep Finer-DBN

Zhengwang Xia<sup>ID</sup>, Tao Zhou, Saqib Mamoon, and Jianfeng Lu<sup>ID</sup>, *Member, IEEE*

**Abstract**—The treatment of neurodegenerative diseases is expensive, and long-term treatment makes families bear a heavy burden. Accumulating evidence suggests that the high conversion rate can possibly be reduced if clinical interventions are applied at the early stage of brain diseases. Thus, a variety of deep learning methods are utilized to recognize the early stages of neurodegenerative diseases for clinical intervention and treatment. However, most existing methods have ignored the issue of sample imbalance, which often makes it difficult to train an effective model due to lack of a large number of negative samples. To address this problem, we propose a two-stage method, which is used to learn the compression and recover rules of normal subjects so that potential negative samples can be detected. The experimental results show that the proposed method can not only obtain a superb recognition result, but also give an explanation that conforms to the physiological mechanism. Most importantly, the deep learning model does not need to be retrained for each type of disease, which can be widely applied to the diagnosis of various brain diseases. Furthermore, this research could have great potential in understanding regional dysfunction of various brain diseases.

**Index Terms**—Alzheimer’s disease (AD), deep learning, fMRI classification, sample imbalance.

## I. INTRODUCTION

ALZHEIMER’S disease (AD), a progressive, irreversible neurodegenerative disease, is the most common type of dementia, which accounts for 50% to 80% of dementia cases [1]. As reported, the incidence of AD doubles every five years after age 65, and 1 in 85 people will be affected by this disease by 2050 [2]. Since there is no effective treatment for AD, the timely and accurate identification of AD and its intermediate stage (i.e., Mild Cognitive Impairment (MCI)) is particular important [3], [4].

Functional magnetic resonance imaging (fMRI) [5], a powerful noninvasive technique for detecting brain activities, provides unprecedented opportunities for dementia

research. Due to the high-dimensional nature of neuroimaging data, existing methods usually use functional partition templates (i.e., automated anatomical labeling (AAL) template [6]) or select region-of-interest (ROI) to conduct research on brain functional interaction patterns, and build brain network models to detect brain disease biomarkers. For example, Szewczyk-Krolikowski *et al.* used independent component analysis (ICA) and dual regression to construct brain functional network, discovering reduced connectivity between the basal ganglia network and widespread frontal, temporal, parietal cortical regions in patients compared with healthy controls [7]. Gorges *et al.* conducted a seed-to-seed approach to resting-state fMRI default mode network (DMN) analysis, founding reduced functional connectivity between the medial prefrontal cortex (PFC) and the posterior cingulate cortex (PCC) in Parkinson’s disease patients [8]. In addition, Chen *et al.* introduced a sliding time-window method to assess dynamic connectivity changes process between healthy controls (HCs) and AD, and various unique and additional biomarkers of disorders are observed which cannot be detected with static functional connectivity measures [9]. However, most of the current machine learning paradigms rely on these manually designed brain networks to detect biomarkers of brain diseases, such as default mode network [10], Pearson’s correlation network [9], and sparse brain network [11]. These manually designed brain models may not fully reflect the actual laws of brain interaction patterns.

A large number of research results have proved that, compared with traditional manually-designed brain functional network models, deep neural networks have unparalleled advantages in fMRI data characterization and modeling [12], [13]. In the field of assisted diagnosis of brain disease, Wang *et al.* designed a novel VGG-based attention network to recognize AD, which can realize accurate diagnosis with various data augmentation methods [14]. Li *et al.* constructed a dual-branch convolution neural network (CNN) to extract finer features of hippocampal regions to predict the individual subject’s progression of MCI to AD, and obtained roughly consistent results with clinical data [15]. Wang *et al.* proposed a new AD detection approach based on a single slice. This method adopted the multilayer perceptron, and finally the accuracy reached 92.4% [16]. In the field of brain function decoding, Cui *et al.* used a novel deep recurrent neural network to model brain functional networks from task fMRI data, experimental results showed that the proposed model can not only reconstruct brain functional networks, but also identify more meaningful brain networks under multiple time scales [17]. Dong *et al.* adopted a novel sparse deep belief network (VS-DBN) for modeling the hierarchical brain networks from

Manuscript received May 19, 2021; revised July 26, 2021; accepted September 7, 2021. Date of publication September 10, 2021; date of current version September 24, 2021. This work was supported by the National Natural Science Foundation of China under Grant 62172228. (Corresponding author: Jianfeng Lu.)

This work involved human subjects or animals in its research. Approval of all ethical and experimental procedures and protocols was granted by the Research Ethics Board of ADNI and PPMI (see <http://adni.loni.usc.edu/study-design/ongoing-investigations/> and <https://www.ppmi-info.org/study-design/>).

The authors are with the School of Computer Science and Engineering, Nanjing University of Science and Technology, Nanjing 210094, China (e-mail: xzhengwang@njust.edu.cn; taozhou.ai@gmail.com; saqi\_hawk@yahoo.com; lujf@njust.edu.cn).

Digital Object Identifier 10.1109/TNSRE.2021.3111989

volumetric fMRI data and demonstrated that a large number of interpretable and meaningful brain network can be robustly reconstructed in a hierarchical fashion [18].

The aforementioned methods have confirmed the excellent feature extraction and activity decoding capabilities of deep neural networks. However, these case-driven methods ignore the problem of sample imbalance, which is the most common phenomenon in the domain of biomedical image analysis. Currently, deep unsupervised representation learning has produced new methods in the field of Unsupervised Anomaly Detection (UAD). The main principle of the work is to obtain a good feature representation by learning to compress and recover HCs, so that potential negative samples (e.g., MCI) with abnormal structures can be detected from erroneous recoveries. For instance, Baur *et al.* used unsupervised auto-encoder to model the brain structure of HCs and found that trained model can effectively isolate potential pathological structural abnormalities [19]. Zhao *et al.* proposed a defect detection model based on positive sample training without manual label. The model can automatically repair defects in regular pattern texture images and give specific locations of defects [20]. However, features extracted by unsupervised representation learning model (e.g., deep belief network (DBN)) are coarse, and may not be able to detect subtle texture changes [19].

Generally, the application of deep learning in neuroimaging analysis still suffers from the following challenges. First, supervised deep learning methods (such as CNN) usually require a large number of positive and negative paired samples for training. However, due to personal privacy, low disease incidence, etc., the number of samples for certain diseases may be very scarce. Second, although unsupervised representation learning methods (such as auto-encoders) can be trained without negative samples. However, the coarse-grained features extracted by them are not conducive to the recognition of subtle changes. Third, it is believed that the brain is hierarchically organized [18], [21], while many existing methods cannot well represent the spatial hierarchical relationship of brain.

To overcome these challenges, we propose a novel dementia recognition framework via finer deep belief network (Finer-DBN), which can simultaneously extract coarse-grained and fine-grained features for HCs' data reconstruction. At the same time, the network model stacked with basic modules can well represent the hierarchical relationship of brain functions. Specifically, we design a new basic module called ConvRBM. The brain signal will be input into two branches at the same time, one is 1D convolution for extracting fine-grained features, and the other is the Restricted Boltzmann Machine (RBM) for extracting coarse-grained features. It is worth noting that the data we input is voxel-level data of a single volume, not time series data along the time dimension. On the one hand, it is more convenient to study the spatial hierarchical relationship of brain functions by encoding volume signal; on the other hand, a single volume of standard template brain has the same amount of voxel data, so the training and testing of our model will not require the subjects to have the same sampling time, which will have a broader prospect in practical application.

In summary, our proposed model has the following advantages: (1) it relieves the need of vast amounts of negative

samples for training deep learning models; (2) it can detect arbitrary, even rare pathological lesions which may not be detected by supervised methods (lesions are not included in the training set) in theory; (3) it can characterize the spatial hierarchical relationship of brain; (4) it is universal and does not need to train different deep learning models for different diseases.

The rest of this paper is organized as follows. In Materials and Methods section, we introduce the proposed framework for dementia recognition. Then, we describe experimental results in Results and Discussion section. Finally, we conclude this study in Conclusion section.

## II. MATERIALS AND METHODS

### A. Proposed Framework

The Fig. 1 provides an overview of the proposed framework. Our objective is to predict the cognitive physiological state of each individual. In fact, the framework belongs to a two-stage method which firstly generates representation features and then uses features during identification. Specifically, the first stage corresponds to the steps of Fig. 1 (a)-(c), the objective is to gain a good feature representation of normal subjects by training the Finer-DBN network with normal subjects' data [19], [20]. The second stage corresponds to the steps of Fig. 1 (d)-(e), which is to recognize the dementia cases. At this stage, we will first input the data of all subjects (including normal subjects and subjects with brain diseases) into the Finer-DBN network trained in the first stage to extract features. Then, we will only need to retrain the subsequent classifiers for different types of disease, and do not need to retrain the deep learning model, which undoubtedly has greater advantages than previous supervised learning methods. The detailed training steps can be seen from Section III (Model Training and Complexity).

### B. Data Acquisition and Processing

In this study, a total of 334 subjects' resting state fMRI data from the publicly available Alzheimer's disease neuroimaging initiative (ADNI) project and Parkinson's Progression Markers Initiative (PPMI) are used for testing the proposed framework, including normal controls (NC), early MCI (eMCI), late MCI (LMCI), Prodromal (Prod), GenCohortUnaff (GenUf) and GenCohortPD (GenPD). (For more details about imaging parameters, please see the ADNI protocols at <http://adni.loni.ucla.edu> and PPMI protocols at <http://www.ppmi-info.org/>), and the detailed information is shown in Table I.

For fMRI data preprocessing, we apply the standard procedures as follows. First, for magnetization equilibrium, the first 5 volumes of each subject were discarded before preprocessing, and then the remaining volumes were involved in the subsequent pipeline (<https://web.conn-toolbox.org/>), was used to perform functional realignment, motion estimation, slice-timing correction, outlier detection [22], direct segmentation and normalization and functional smoothing with a Gaussian kernel of 8mm full width half maximum (FWHM), etc. Finally, all subjects are normalized to the Montreal Neurological Institute's (MNI) 152 space with 2mm spatial resolution, each volume contains 228,453 voxels.

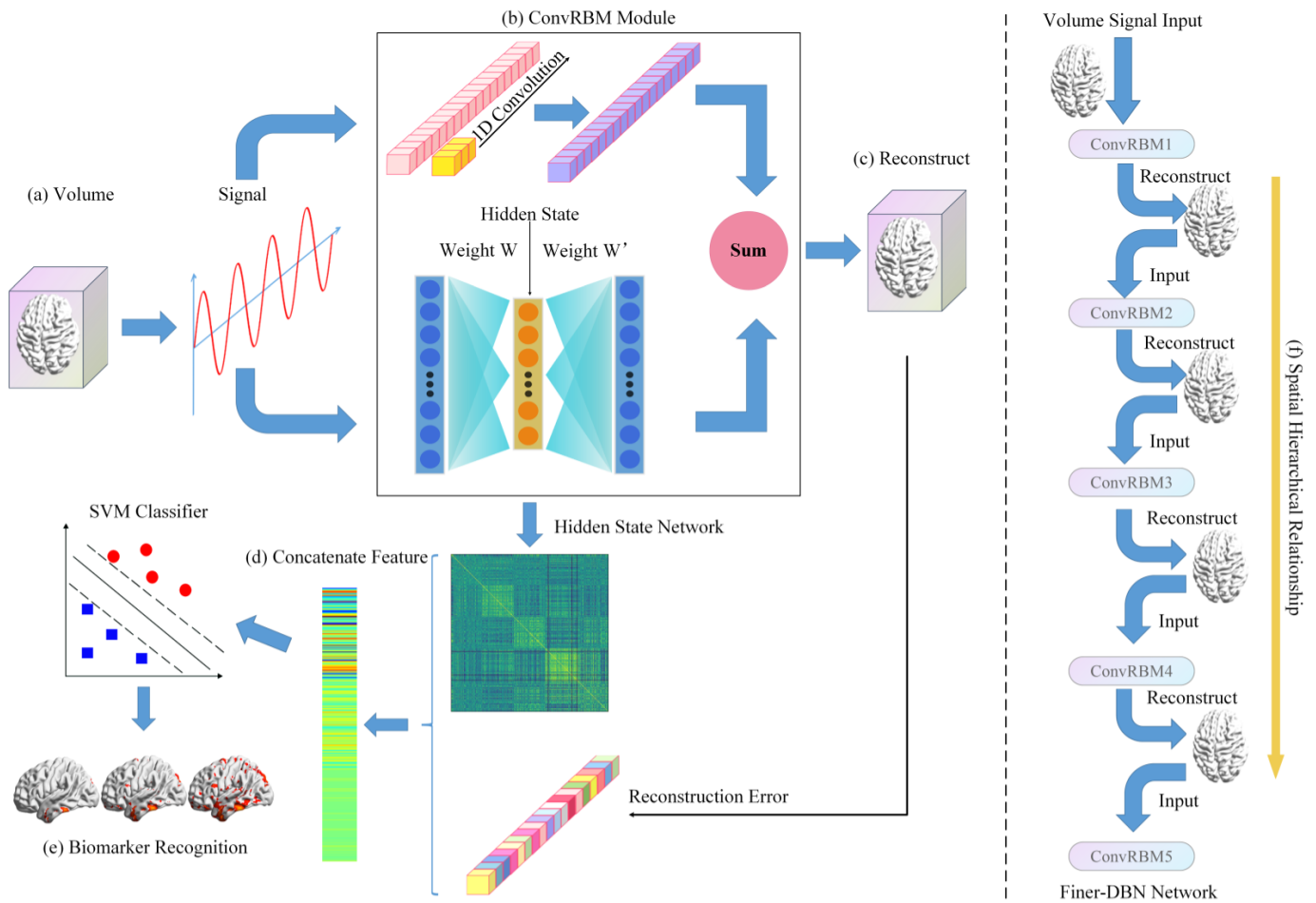


Fig. 1. Illustration of recognizing dementia with Finer-DBN. (a) Each preprocessed fMRI volume data was treated as a single training sample for Finer-DBN network. (b) The basic module that constitutes the Finer-DBN. It contains two branches for accepting input and extracting features. (c) Reconstruct the brain volume data by fusing the outputs of two branches of ConvRBM module. (d) Concatenate the coarse-grained (clustering coefficient of hidden state network) and fine-grained (reconstruction error) features for training classifier. (e) Visualize biomarkers at all stages of dementia into standard brain space. (f) Analyze the spatial distribution relationship between the features extracted by different ConvRBM modules.

TABLE I  
DETAILED INFORMATION ABOUT THE USED DATASET

| Group         | NC <sup>1</sup> | eMCI     | LMCI     | NC <sup>2</sup> | Prodromal | GenCohortUnaff | GenCohortPD |
|---------------|-----------------|----------|----------|-----------------|-----------|----------------|-------------|
| Male/Female   | 28/39           | 32/45    | 50/20    | 18/4            | 32/9      | 12/25          | 12/8        |
| Age(mean±STD) | 74.1±6.2        | 71.2±6.9 | 71.2±8.3 | 64.4±9.4        | 69.8±5.4  | 61.8±7.6       | 65.4±5.7    |

Note. NC<sup>1</sup>: NC group data of ADNI dataset; NC<sup>2</sup>: NC group data of PPMI dataset

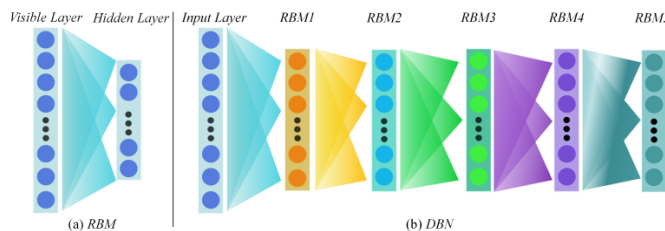


Fig. 2. Schematic illustration of RBM and DBN.

### C. RBM

Restricted Boltzmann Machine (RBM), a generative model with two layers: visible layer and hidden layer (Fig. 2), can approximate the potential probability distribution of training data. RBM can also be interpreted as an undirected probability

graphical model [23], in which the state of the visible layer and the state of the hidden layer can affect each other. The visible layer for accepting observations is fully connected to the hidden layer for extracting features [24], while the connections are yet to be established within the visible layer and hidden layer. The joint probability distribution of visible layer  $\mathbf{v}$  and hidden layer  $\mathbf{h}$  is defined as:

$$P(\mathbf{v}, \mathbf{h}) = \frac{1}{Z} \exp(-E(\mathbf{v}, \mathbf{h})) \quad (1)$$

where  $Z$  is the sum of  $e^{-E(\mathbf{v}, \mathbf{h})}$ ,  $E$  is an energy function. The energy function has different definitions under different data distributions. When the visible layer and the hidden layer are both binary distributions, Bernoulli-Bernoulli  $E(\mathbf{v}, \mathbf{h})$  is generally used; when the visible layer is real-valued data

and the hidden layer is binary, Gaussian-Bernoulli  $E(\mathbf{v}, \mathbf{h})$  is applied. In the context of fMRI data, the activation of each voxel is real-valued data and in Gaussian distribution. Thus, Gaussian-Bernoulli  $E(\mathbf{v}, \mathbf{h})$  is adopted as the energy function [25] and the detailed definition is as follows:

$$E(\mathbf{v}, \mathbf{h}) = - \sum_i \sum_j \frac{v_i}{\sigma_i} w_{i,j} h_j - \sum_i \frac{(b_i - v_i)^2}{\sigma_i^2} - \sum_j c_j h_j \quad (2)$$

where  $v_i$  represents the signal strength value at the  $i$ -th position of each volume,  $h_j \in \{0, 1\}$ ,  $\sigma_i$  is the standard deviation of  $i$ -th visible neuron,  $w_{i,j}$  is the weight between  $v_i$  and  $h_j$ ,  $b_i$  is the bias of the  $i$ -th visible neuron, and  $c_j$  is the bias of the  $j$ -th hidden neuron.

The conditional distribution of  $P(\mathbf{h}|\mathbf{v})$  and  $P(\mathbf{v}|\mathbf{h})$  is given by

$$P(h_j = 1|\mathbf{v}) = \text{sigmoid}\left(\sum_i w_{i,j} v_i + c_j\right) \quad (3)$$

$$P(v_i = 1|\mathbf{h}) = \text{sigmoid}\left(\sum_j w_{i,j} h_j + b_i\right) \quad (4)$$

where the mathematical definition of sigmoid is  $1/(1 + \exp(-x))$ .

RBM was trained to maximize the log-likelihood of visible neurons  $\mathbf{v}$ , the probability of visible neurons  $\mathbf{v}$  inferred from the model is

$$P(\mathbf{v}) = \sum_h \exp(-E(\mathbf{v}, \mathbf{h})) / \sum_v \sum_h \exp(-E(\mathbf{v}, \mathbf{h})) \quad (5)$$

To update the model, the results from the log probability regarding the weights are as follows

$$\partial \log P(\mathbf{v}) / \partial w_{i,j} = \langle v_i h_j \rangle - \langle v_i h_j \rangle_{\text{model}} \quad (6)$$

The update rule for the weights follows the gradient of the log likelihood is

$$\Delta w_{i,j} = \alpha (\langle v_i h_j \rangle_{\text{data}} - \langle v_i h_j \rangle_{\text{model}}) \quad (7)$$

where  $\alpha$  is the learning rate. However, it takes exponential time to calculate the exact value of the term  $\langle v_i h_j \rangle_{\text{model}}$ . The contrastive divergence (CD) [26] algorithm can be used to approximate the gradient to complete the calculation. The new update rule can be set as

$$\Delta w_{i,j} = \alpha (\langle v_i h_j \rangle_{\text{data}} - \langle v_i h_j \rangle_{\text{recon}}) \quad (8)$$

where the term  $\langle v_i h_j \rangle_{\text{recon}}$  represents the expectation of reconstructions generated by initializing the data from the hidden neurons and then updating the hidden neurons according to the visible layer data.

#### D. ConvRBM

Modeling fMRI with temporal features has already been explored in massive literature [27], [28]. However, the inter-subject variability is more associated with the volatile time courses rather than the spatial volumes under different imaging sessions. In this case, it appears that taking volumes as input possibly works better than time series in eliminating the inter-subject variability factors [29]. In this paper, a volumetric learning scheme was applied where each volume from the fMRI data was taken as a sample. Thus, after preprocessing, the volumes of all subjects were concatenated along

time dimension and shuffled for further group-wise training. As shown in Fig. 1(a), each fMRI volume at a time point was used as a training sample and the Finer-DBN was trained in an unsupervised fashion.

In addition, in order to obtain more refined features, we designed a novel basic module ConvRBM for reconstructing fMRI data. As shown in Fig. 1(b), it is a dual-branch structure module, including a 1D convolution branch and an RBM branch to extract features from the input data simultaneously. Specifically, the dimension of the input data is 228,453, which corresponds to the number of voxels in MNI-152 space of 2mm spacing. The 1D convolution branch is constructed by a convolution layer with kernel size 3, yielding outputs with the same size of input by padding operation. The visible layer of RBM model is constructed with 228,453 nodes, and hidden layer nodes are set as 100 based on previous prior knowledge [18], [30]. The parameters of weight  $\mathbf{W}$  and weight  $\mathbf{W}'$  are shared, where  $\mathbf{W}'$  is the transpose of  $\mathbf{W}$ .

The reasons for using this structure can be explained from the following three aspects. First of all, the form of data input in our method is the brain volumetric signal, which is a vector. Therefore, the 1D convolution structure is more compatible with the form of the input data. Secondly, convolution is widely used for feature extraction. We maintain the input and output sizes consistent in order to avoid losing subtle information during the process of extracting features. Finally, because the parameters of RBM are optimized by the principle of maximum likelihood estimation, it is more attractive in terms of model interpretability [23].

#### E. Model Training and Complexity

The framework is a two-stage method and the specific implementation process for dementia identification can be divided into the following three steps:

- train the Finer-DBN network with the data of normal subjects;
- input the data of all subjects (including normal subjects and subjects with brain diseases) into the Finer-DBN model trained in the previous step to extract features;
- train different classifiers for identifying different types of disease;

The first stage corresponds to the first step of the execution process, and the objective is to obtain the feature representation of volumetric data. The second stage corresponds to the last two steps during the execution process. The main principle of the proposed method is to obtain the feature representation by learning to compress and recover volumetric data of normal subjects, so that potential negative samples (e.g., dementia cases) with abnormal data distribution can be detected from erroneous recoveries. In general, the biggest difference between the proposed method and the traditional deep learning method is that the feature extraction and classification are divided into two stages and executed separately. Relatively speaking, our method may be more suitable for practical application. For example, we want to judge whether a subject is healthy or suffering from a certain disease. In the traditional CNN-based method, we may need to input sample data into various disease detection models (such as AD detection model, MCI detection model, Parkinson's detection model) before we can conclude that the sample is healthy or has a certain disease.

TABLE II  
TIME AND SPACE COMPLEXITY OF DBN AND FINER-DBN

|           | FLOPs  | byte    |
|-----------|--------|---------|
| DBN       | 216.8M | 110.05M |
| Finer-DBN | 220M   | 114.4M  |

But it is almost impossible to obtain diagnosis models for all diseases. In contrast, our method is to directly judge whether the sample is healthy or not according to the difference between the reconstructed data and the original data, and does not need to go through the testing of multiple models.

The deep learning model Finer-DBN is implemented by the tensorflow framework. The optimizer adopts the Adam optimizer with a learning rate of 0.001 and a batchsize of 4, and the epoch is set as 50. The detailed training steps of Finer-DBN are as follows:

Finer-DBN is a hierarchical structure composed of multiple stacked ConvRBM modules. First, train the first ConvRBM module based on the sample-normalized volumetric data of all normal subjects. Next, fix the parameters of the first ConvRBM module and use the output of the first ConvRBM as the input of the second ConvRBM module. Then, train the second ConvRBM module with the first ConvRBM output. By analogy, after fixing the parameters of the previous layer is obtained for the input of the next layer. Finer-DBN repeats the above training process for each sample in layer-wise fashion. Specifically, each ConvRBM module was gradually optimized by minimizing the error between the original data and the reconstructed data, that is

$$\text{loss}_i = \text{MSE}(y_i - x_i), \quad i \in \{1, 2, 3, 4, 5\} \quad (9)$$

where  $\text{MSE}$  is the mean-squared loss.  $x_i$  is the input of  $i$ -th ConvRBM module, and  $y_i$  is the output of  $i$ -th ConvRBM module.

After finishing Finer-DBN training, the support vector machine (SVM) [31] with RBF kernel was introduced as the classifier for disease identification. SVM seeks a maximum margin hyperplane to separate the samples of one class from those of the other class. The empirical risk on training data and the complexity of the model can be balanced by the hyperparameter  $C$ , thereby ensuring good generalization ability on unseen data. In this work, we use 10-fold cross-validation strategy to evaluate the generalization performance of SVM classifier. As the performance of SVM classifier (RBF kernel) is dependent on the hyperparameters  $C$  and  $\gamma$ . We use a nested 10-fold cross-validation procedure to determine optimal values for the two hyperparameters in the following ranges:  $C \in [0.1, 0.2, \dots, 1.0]$ ,  $\gamma \in [0.1, 0.2, \dots, 1.0]$ .

Based on the algorithm training process of DBN and Finer-DBN, we derive their total floating point operations (FLOPs) and space complexity for each iteration, the detailed information is shown in Table II. The 1D convolution branch leads to a slight increase of time complexity (approximately 1.48%) and space complexity (approximately 3.95%).

#### F. Feature Extraction and Evaluation Criteria

The dual-branch ConvRBM module extracts two types of features, which RBM branch is used for coarse-grained feature extraction and 1D convolution branch is used for fine-grained

voxel-level feature extraction. For each subject, the hidden layer outputs  $\mathbf{h} \in R^{t \times N}$  of the RBM branch can be obtained, where  $t$  represents the time points of data acquisition, and  $N$  is the number of neurons in the hidden layer. We regard each neuron in the hidden layer as a node, and then construct the correlation matrix hidden state network (Fig. 1(c),  $\text{HSN} \in R^{N \times N}$ ) to characterize the temporal-interaction between neurons in the same layer. The results of a large number of previous studies have proved that the clustering coefficient has great advantages in characterizing brain network differences, and has been widely used as the core feature in the classification of neurological diseases [32]–[34]. Thus, we extract the clustering coefficients of HSN to act as the coarse-grained features, the specific definition is as follows:

$$C = \frac{1}{N} \sum_{i=1}^N \frac{2E_i}{d_i(d_i - 1)} \quad (10)$$

where  $N$  is the number of nodes in the hidden layer,  $d_i$  is the degree of node  $i$ ,  $E_i$  is the number of edges connected to node  $i$ . In addition, we treat the input and output reconstruction errors of the corresponding ConvRBM module of each subject as fine-grained features, and finally obtain voxel-level features with a size of  $t \times 228, 453$ .

To quantitatively evaluate the performance of the Finer-DBN framework in recognizing dementia disease, accuracy (ACC), sensitivity (SEN), specificity (SPE), and F1 score [35] were calculated based on 10-fold cross-validation to increase the confidence level of the recognition results. Before giving the specific definition of the above evaluation criteria, it is necessary to introduce the following definitions:

Positive samples: subjects from NC

Negative samples: subjects from eMCI or LMCI or other dementia disease

- True positive (TP): the number of subjects correctly labeled positive samples
- True negative (TN): the number of subjects correctly labeled negative samples
- False positive (FP): the number of negative samples incorrectly labeled as positive samples
- False negative (FN): the number of positive samples incorrectly labeled as negative samples

Based on the above definitions, ACC, SEN, SPE and F1 score can be defined as:

$$\text{ACC} = \frac{TP + TN}{TP + TN + FP + FN} \quad (11)$$

$$\text{SEN} = \frac{TP}{TP + FN} \quad (12)$$

$$\text{SPE} = \frac{TN}{TN + FP} \quad (13)$$

$$\text{F1score} = \frac{2 \times TP}{2 \times TP + FP + FN} \quad (14)$$

#### G. Spatial Hierarchical Relationship

In order to interpret the features learned by Finer-DBN, we need to map out which areas of the brain help to distinguish different dementia stages. There are several ways [36]–[38] to visualize a deep neural network, we choose the most commonly used layer activation method [36] for visualization

TABLE III  
RECOGNITION PERFORMANCE OF DIFFERENT MODELS IN OUR NINE TASKS

| Model                  | NC <sup>1</sup> vs. eMCI |              |              |              | NC <sup>1</sup> vs. LMCI  |              |              |              | eMCI vs. LMCI             |              |              |              |
|------------------------|--------------------------|--------------|--------------|--------------|---------------------------|--------------|--------------|--------------|---------------------------|--------------|--------------|--------------|
|                        | ACC                      | SEN          | SPE          | F1           | ACC                       | SEN          | SPE          | F1           | ACC                       | SEN          | SPE          | F1           |
| DBN <sup>1</sup>       | 72.29                    | 76.53        | 69.26        | 70.57        | 73.00                     | 75.20        | 71.39        | 71.01        | 75.86                     | 74.56        | 77.71        | 74.43        |
| DBN <sup>2</sup>       | 67.21                    | 71.08        | 64.43        | 63.86        | 67.92                     | 70.30        | 65.35        | 66.24        | 69.43                     | 68.11        | 69.75        | 68.33        |
| DBN <sup>3</sup>       | 68.79                    | 70.00        | 66.89        | 66.27        | 72.23                     | 73.44        | 70.83        | 70.45        | 75.64                     | 73.64        | 79.02        | 75.21        |
| Finer-DBN <sup>1</sup> | <b>78.36</b>             | <b>80.54</b> | <b>77.43</b> | <b>76.00</b> | <b>79.69</b>              | 79.83        | <b>79.06</b> | <b>77.98</b> | <b>81.00</b>              | <b>78.86</b> | <b>83.80</b> | <b>80.59</b> |
| Finer-DBN <sup>2</sup> | 71.86                    | 72.66        | 71.29        | 68.58        | 74.00                     | 75.41        | 71.73        | 71.93        | 75.79                     | 74.84        | 77.45        | 75.48        |
| Finer-DBN <sup>3</sup> | 75.07                    | 76.89        | 73.90        | 72.95        | 78.23                     | <b>81.73</b> | 74.95        | 76.93        | 79.00                     | 75.93        | 83.59        | 78.87        |
| Model                  | NC <sup>2</sup> vs. Prod |              |              |              | NC <sup>2</sup> vs. GenUf |              |              |              | NC <sup>2</sup> vs. GenPD |              |              |              |
|                        | ACC                      | SEN          | SPE          | F1           | ACC                       | SEN          | SPE          | F1           | ACC                       | SEN          | SPE          | F1           |
| DBN <sup>1</sup>       | 67.38                    | 70.35        | 66.34        | 67.72        | 69.18                     | 68.54        | 70.26        | 67.96        | 71.94                     | 69.87        | 74.40        | 70.48        |
| DBN <sup>2</sup>       | 71.29                    | 70.89        | 72.14        | 70.53        | 71.47                     | 71.39        | 71.25        | 70.73        | 73.13                     | 68.88        | 77.65        | 71.34        |
| DBN <sup>3</sup>       | 68.82                    | 69.99        | 68.00        | 68.47        | 71.29                     | 69.92        | 72.93        | 68.71        | 73.94                     | 69.48        | 78.47        | 72.16        |
| Finer-DBN <sup>1</sup> | 70.59                    | 71.06        | 69.96        | 68.99        | 73.12                     | 72.57        | 74.20        | 72.18        | 74.47                     | 76.84        | 71.70        | 74.91        |
| Finer-DBN <sup>2</sup> | <b>75.47</b>             | <b>77.91</b> | <b>73.14</b> | <b>75.04</b> | 77.24                     | 77.91        | <b>76.97</b> | 75.59        | 77.31                     | 74.28        | 79.39        | 76.34        |
| Finer-DBN <sup>3</sup> | 72.59                    | 73.41        | 71.82        | 71.44        | <b>78.35</b>              | <b>79.95</b> | 76.25        | <b>78.90</b> | <b>78.69</b>              | <b>78.50</b> | <b>79.52</b> | <b>78.56</b> |
| Model                  | Prod vs. GenUf           |              |              |              | Prod vs. GenPD            |              |              |              | GenUf vs. GenPD           |              |              |              |
|                        | ACC                      | SEN          | SPE          | F1           | ACC                       | SEN          | SPE          | F1           | ACC                       | SEN          | SPE          | F1           |
| DBN <sup>1</sup>       | 74.40                    | 77.27        | 70.58        | 75.12        | 75.69                     | 77.55        | 73.83        | 75.30        | 75.44                     | 77.58        | 73.33        | 74.81        |
| DBN <sup>2</sup>       | 76.00                    | 79.66        | 73.22        | 75.94        | 77.56                     | 79.24        | 76.42        | 76.01        | 77.63                     | 79.26        | 76.04        | 77.00        |
| DBN <sup>3</sup>       | 74.47                    | 76.84        | 71.70        | 74.91        | 77.00                     | 80.00        | 72.69        | 75.95        | 77.38                     | 80.02        | 74.32        | 77.21        |
| Finer-DBN <sup>1</sup> | 78.67                    | 78.28        | 80.10        | 78.00        | 78.94                     | 80.98        | 76.94        | 78.44        | 76.63                     | 80.30        | 73.73        | 76.73        |
| Finer-DBN <sup>2</sup> | <b>80.57</b>             | <b>83.90</b> | <b>80.35</b> | <b>80.20</b> | 80.25                     | <b>81.86</b> | 77.62        | <b>79.97</b> | 77.88                     | <b>80.32</b> | 75.29        | 76.20        |
| Finer-DBN <sup>3</sup> | 79.67                    | 82.75        | 77.12        | 79.52        | <b>81.06</b>              | 81.44        | <b>80.19</b> | 79.88        | <b>78.38</b>              | <b>79.92</b> | <b>77.58</b> | <b>78.04</b> |

Note. <sup>1</sup>: model trained with ADNI NC data; <sup>2</sup>: model trained with PPMI NC data; <sup>3</sup>: model trained with fusion NC data from ADNI and PPMI dataset; NC<sup>1</sup>: NC group data of ADNI dataset; NC<sup>2</sup>: NC group data of PPMI dataset.

due to its easy implementation and generalization. The basic idea is if the input is relevant, a slight variation will cause high change in the layer activation. This can be characterized by the gradient of the output given the input, the positive gradients indicate that a minor change to the input signals increases the output value. To visualize the gradients, we add small perturbation to the raw fMRI data to observe the gradient change of the reconstruction data, and then reconstruction data gradients will be mapped back into the original 3D brain image space, which is the inverse operation of masking in preprocessing steps.

To compare the activation maps derived by Finer-DBN different layers, the spatial overlap rate is defined to measure the similarity of layer-wise activation maps [18]. The specific definition of overlap rate (OR) is as follows:

$$OR(M^i, M^j) = \frac{\sum_{v=1}^N |M_v^i \cap M_v^j|}{\sum_{v=1}^N |M_v^i \cup M_v^j|} \quad (15)$$

where  $M^i$  is the  $i$ -th layer activation map,  $N$  is the number of voxels of standard brain space.

### III. RESULTS

#### A. Recognition Results

We evaluate the proposed method on the ADNI and PPMI database with a 10-fold cross-validation strategy. The trained model not only should be tested on the corresponding data sets, but also should be used for classification task across data sets. Specifically, the following nine binary classification tasks are conducted: *i.e.*, NC vs. eMCI, NC vs. LMCI, eMCI vs. LMCI, NC vs. Prod, NC vs. GenUf, NC vs. GenPD, Prod vs. GenUf, Prod vs. GenPD and GenUf vs. GenPD.

Table III summarizes the recognition performances of models trained on different datasets, where the best scores are highlighted in bold. It is worth noting that when we evaluate the classification performance of the trained model, we may encounter the problem of imbalanced data category. For example, when we classify the NC of PPMI and Prod of PPMI. The Prod category contains 41 subjects, while the NC category only includes 22 subjects. For this kind of classification task with obvious imbalanced data problem, we will randomly select the same number of samples as another category from the category with more sample size to test and evaluate the model. The above process will be performed ten times and averaged to obtain a relatively fair result. The proposed framework is compared with DBN (Fig. 2(b)) under three different training situations, including model trained with ADNI NC data, model trained with PPMI NC data and that is trained with fusion NC data from ADNI and PPMI. DBN and Finer-DBN set the same training hyper-parameters in all cases to avoid the influence of parameter differences on the model prediction results. Parameters details are as below: the learning rate is 0.001, the number of epochs is 50 and the batch size is 4.

As shown in Table III, compared with DBN, our proposed framework has achieved the best classification performance in all nine tasks. This proves that our model can extract finer features after adding a branch, which can significantly improve the classification performance. It can also be clearly observed that there are still some differences between the same models trained on different data sets for the same classification task. On the one hand, this may be caused by the difference in data acquisition parameters. On the other hand, it may be due to the difference in the data size of the data set. Intuitively, a model trained on the corresponding data set can often obtain better classification performance for the data set, for example, Finer-DBN<sup>1</sup> for ADNI and Finer-DBN<sup>2</sup> for PPMI.

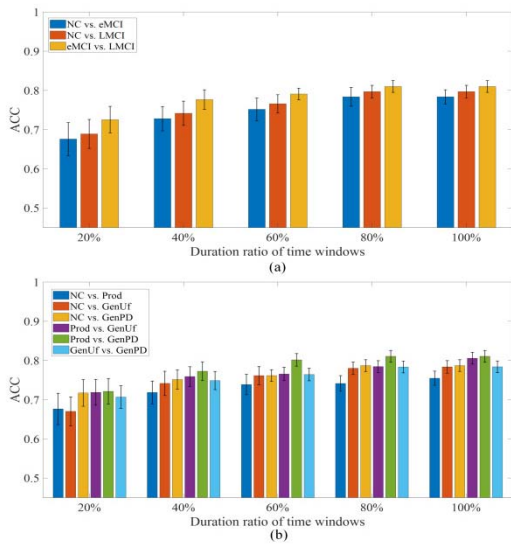


Fig. 3. Effects of Finer-DBN using different time window ratios. (a) The recognition results on ADNI dataset. (b) The recognition results on PPMI dataset.

Secondly, compared with DBN, the gap between the best and worst classification performance of Finer-DBN is smaller on most tasks. It could be attributed to the 1D convolution branch that extracted more features. For different classification tasks, it is not hard to find that the best performance of tasks without NC category is higher than that of tasks with NC category. This demonstrates that different biomarkers may exist in different stages of dementia. There may be fixed imaging differences between NC and dementia cases at a specific stage, while the biomarkers between dementia cases at distinct stages may not be fixed in the same brain regions, resulting in more imaging differences. Thus, it will be more conducive to distinguish cases of dementia at distinct stages. Therefore, those classification tasks that do not include NC category can accomplish superior result.

Finally, we can find that both DBN and Finer-DBN can obtain similar results in cross-data classification tasks. This shows that the design idea of our paper is feasible, that is, a good feature representation can be obtained by learning to compress and reconstruct the data of normal subjects, so that potential negative samples with abnormal data distribution can be detected from the error recovery. The requirement of the classifier SVM for the amount of data is significantly lower than that of deep learning model, which can well solve the problem of sample imbalance. In summary, the superior results in Table III demonstrate the feasibility of our method for dementia recognition.

### B. Ablation Study

The temporal sensitivity of Finer-DBN was evaluated by progressively increasing the duration ratio of fMRI time windows (Fig. 3). It can be seen from Fig. 3(a) and (b) that the classification accuracy of the two data sets (ADNI and PPMI) gradually improves with the increase of the time window ratio, and the standard deviation of the classification effect gradually stabilizes. The main reason possibly that more effective features are drawn from fMRI data with the increase of time window ratio, which promotes the improvement of

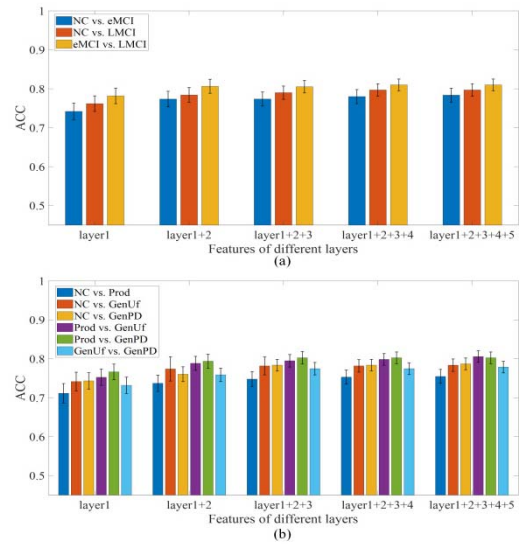


Fig. 4. The Finer-DBN recognition effect by fusing features of different layers. (a) The recognition results on ADNI dataset. (b) The recognition results on PPMI dataset.

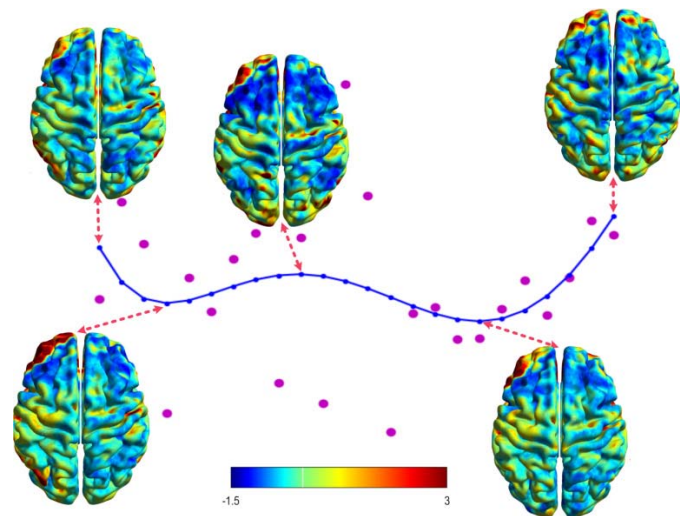


Fig. 5. Brain activation maps of averaged ADNI NC group data learned by Finer-DBN 1<sup>st</sup> layer.

classification effect. The time window ratio rises from 20% to 40%, the classification effect of the two data sets improves fastest, and when the ratio reaches 60%, most classification tasks are very similar to the optimal results. It can still be observed that under different time window ratios, the best performance of tasks without NC category is higher than that of tasks with NC category.

The layer-feature sensitivity of Finer-DBN was also evaluated by fusing the features of different layers (Fig. 4). From Fig. 4(a) and (b), it can be discovered that the classification accuracy of the two datasets (ADNI and PPMI) gradually improves with the increase of the number of fusion feature layers, and the standard deviation of the classification effect gradually tends to be stable. The reason for this may be that higher-level network layer-features can provide extra features, thereby helping to steadily enhance the performance of the classifier. It is also quite easy to find that when the

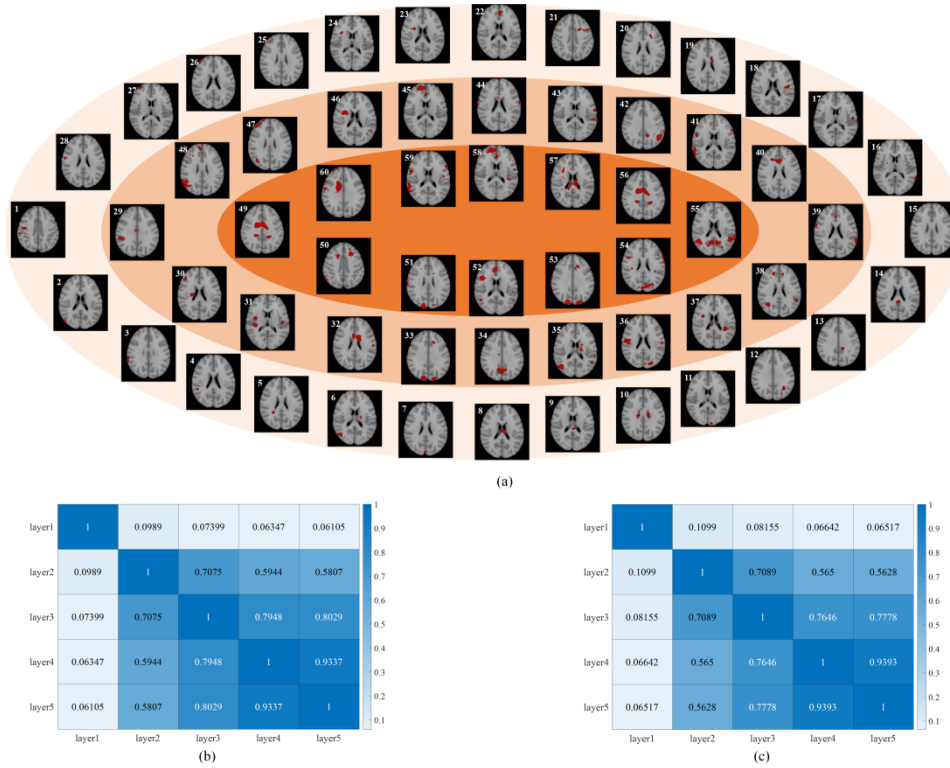


Fig. 6. The hierarchical relationship and spatial similarity of NC group data revealed by Finer-DBN. (a) The hierarchical relationship of brain activation maps. (b) The averaged spatial similarity of ADNI NC group data. (c) The averaged spatial similarity of PPMI NC group data.

first three layers of features are fused, it seems that the classification effect has reached saturation, and there is no significant improvement in the classification effect by adding the features of subsequent layers. It is worth noting that the best performance of tasks without NC category is higher than that of tasks with NC category.

## IV. DISCUSSION

### A. Activation Maps

Besides good classification accuracy, good interpretability is also vital for clinical application. In this section, we randomly intercepted a part of the averaged time series data of the NC group to visualize what Finer-DBN 1<sup>st</sup> layer learned. In Figure 5, purple dots are real fMRI signal data, and the blue line is the signal data reconstructed by Finer-DBN. Meanwhile, brain activation maps at the turning point of the reconstructed curve are also visualized by the layer activation method [36]. These red activated brain regions indicate that the reconstructed value is significantly different from the actual value, the yellow regions represent that there is no significant error between the reconstructed value and the real value, and the blue regions are between the above two.

Comparing these five brain activation maps, we can summarize that the size of the yellow regions does not vary significantly over time, maintaining a relatively stable resting state. However, red regions and the blue regions have relatively large changes, not only in the area of the regions, but also in the intensity of the color. Specifically, the larger real value is, the blue area is larger and the red area is smaller. Meanwhile, the blue area color is darker while the red area is lighter. When the actual value is small, it is just the

opposite of the above phenomenon. As can be viewed, the blue regions are mainly concentrated in the left frontal lobe, part of the right frontal lobe and the right parietal lobe. The red regions with larger reconstruction error are concentrated in the left frontal lobe. Interestingly, we found that these red and blue regions contain many brain regions of the default mode network (DMN) [39], such as posterior cingulate gyrus, right hippocampus, angular gyrus, left inferior temporal gyrus and medial prefrontal lobe. These results demonstrate that the proposed framework not only has excellent data representation ability, but also has good physiological interpretability.

### B. Hierarchy: Spatial Similarity

In this section, we conduct research on the relationship between brain activation maps learned by different network layers, and the specific results are shown in Figure 6. Among them, Fig 6(a) gives the hierarchical relationship between brain activation maps of different layers, Fig 6(b) and Fig 6(c) are the averaged spatial similarity matrix of NC group data in the ADNI and PPMI dataset, respectively. Specifically, we divide the brain into 3 levels according to the spatial similarity index. The basic level is the brain activation map numbered 1-28 in the Fig. 6(a), which corresponds to the features learned by the 1<sup>st</sup> layer of the network. The middle level is the brain activation map numbered 29-48 in the Fig. 6(a), which corresponds to the features learned by the 2<sup>nd</sup> layer of the network. The high-level is the brain activation map numbered 49-60 in the Fig. 6(a), which corresponds to the features learned from the third to the fifth layer of the network. The reason for combing the features of the last three layers into the same level is that there is no obvious difference

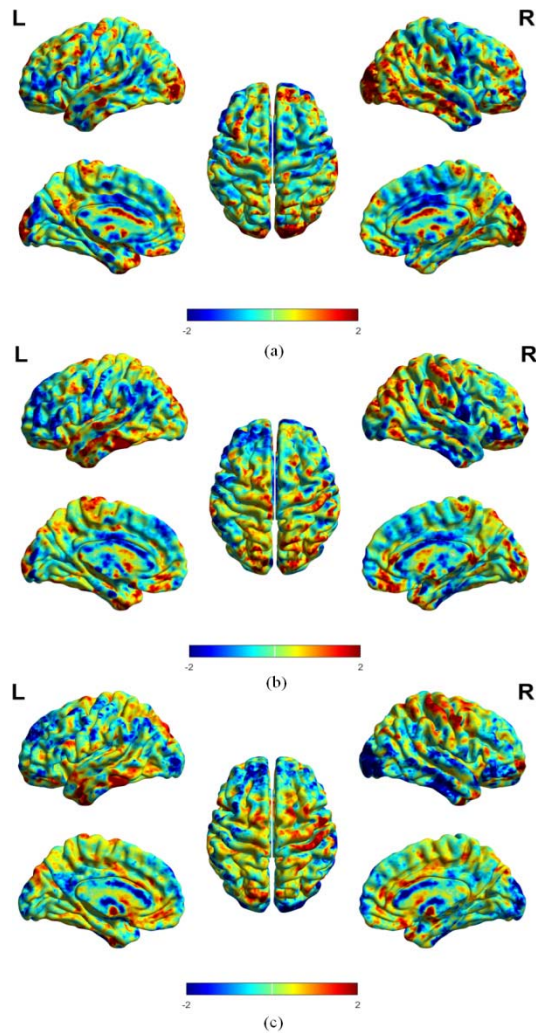


Fig. 7. Dementia-related brain maps of ADNI data. (a) NC vs eMCI. (b) NC vs LMCI. (c) eMCI vs LMCI.

among the features of the 3<sup>rd</sup>, 4<sup>th</sup> and 5<sup>th</sup> layer, and their average spatial similarity is more than 80%.

For the hierarchical relationship, we found that some high-level brain activation maps are comprised of multiple low-level brain activation maps. For example, the 33<sup>rd</sup> brain activation map is composed of the 11<sup>st</sup> and the 20<sup>th</sup> brain activation map, the 42<sup>nd</sup> brain activation map is composed of the 13<sup>rd</sup> and the 15<sup>th</sup> brain activation map and the 51<sup>st</sup> brain activation map is composed of the 33<sup>rd</sup> and the 3<sup>rd</sup> brain activation map. Such phenomenon may indicate that the brain function is organized hierarchically, and the brain may includes many known or unknown basic level activation maps, which are the basic components of higher-order functions. These basic brain activation regions cooperate with each other to complete various complex tasks.

For spatial similarity between features learned by different layers, we give the average spatial similarity matrix of NC group data from different datasets. The two matrices are compatible in many aspects. First, the closer of the two layers are, the larger spatial similarity between them. Second, the higher-level layer has the larger averaged spatial similarity. The reasons for this phenomenon can be accounted for from

two aspects. For one thing, Finer-DBN is trained layer by layer with the output of the shallow layer as the input of the subsequent layer, which makes the spatial similarity between the adjacent layers larger. Secondly, the neurons of the higher-layer composite larger receptive fields, the small changes in local regions may have limited impact on high-level neurons. This may be for the reason that the higher the layer, the higher the averaged spatial similarity.

### C. Dementia-Related Feature Visualization

After multiple encoding and decoding, Finer-DBN can obtain more consistent brain function data by reconstruction. We believe that those regions with great differences between different types of reconstruction data play a major role in the classification task between them. Figure 7 gives the dementia-related visualization results, where the red and blue regions have greater influence on their classification results.

Comparing the results of the three images, we can note that the left prefrontal lobe and occipital lobe have always played important roles in the classification task at each stage. In the early stage of dementia, the difference in the right hippocampus is not significant, but in the late stage of dementia, the importance of the right hippocampus increased significantly compared with the early stage. Therefore, the right hippocampus may be a very effective biomarker in identifying the stage of dementia. The above research results are basically consistent with the results of many previous studies [4], [9], [40], reflecting that our model not only has good data characterization abilities, but also has excellent interpretability.

## V. CONCLUSION

In this paper, we proposed a novel dementia recognition framework based on the Finer-DBN. With massive experiments across datasets, the Finer-DBN model shows its promising capability of characterizing fMRI data under a hierarchical structure. Feature visualization based on the layer activation method validated that activation maps learned by Finer-DBN are meaningful and can be well interpreted. With the layer at higher levels in the Finer-DBN structure, the activated brain regions tend to be large and the reconstructed data of the same category is more consistent. It can be observed that some basic-level brain activation maps merge into higher-level brain activation maps, which indeed suggests the hierarchical architecture of brain function. Besides, the experimental results show that the left prefrontal lobe and occipital lobe play an important role in discriminating dementia at all stages. Moreover, the right hippocampus may be very effective as a biomarker to determine the stage of dementia. In the future work, we will apply the proposed model to more auto-encoder networks, and further investigate the specific relationship of activation maps between different hierarchical levels. Furthermore we will focus on interpreting the corresponding neuroscientific meanings of the hierarchical organization of the brain functions in both healthy and diseased brains.

### ACKNOWLEDGMENT

Data used in preparation of this article were obtained from Alzheimer's Disease Neuroimaging Initiative (ADNI) database ([www.loni.ucla.edu/ADNI](http://www.loni.ucla.edu/ADNI)). As such, the investigators within

the ADNI contributed to the design and implementation of ADNI and/or provided data but did not participate in analysis or writing of this report. A complete listing of ADNI investigators can be found at: [www.loni.ucla.edu/ADNI/Collaboration/ADNI\\_Authorship\\_list.pdf](http://www.loni.ucla.edu/ADNI/Collaboration/ADNI_Authorship_list.pdf).

## REFERENCES

- [1] Alzheimer's Association, "2016 Alzheimer's disease facts and figures," *Alzheimer's Dementia*, vol. 12, no. 4, pp. 459–509, Apr. 2016.
- [2] GBD 2016 Dementia Collaborators, "Global, regional, and national burden of Alzheimer's disease and other dementias, 1990–2016: A systematic analysis for the global burden of disease study 2016," *Lancet Neurol.*, vol. 18, no. 1, pp. 88–106, Jan. 2019.
- [3] Z. Long *et al.*, "A support vector machine-based method to identify mild cognitive impairment with multi-level characteristics of magnetic resonance imaging," *Neuroscience*, vol. 331, no. 7, pp. 169–176, 2016.
- [4] T. Zhou, K.-H. Thung, M. Liu, F. Shi, C. Zhang, and D. Shen, "Multi-modal latent space inducing ensemble SVM classifier for early dementia diagnosis with neuroimaging data," *Med. Image Anal.*, vol. 60, Feb. 2020, Art. no. 101630.
- [5] R. Jalilianhasanpour, E. Beheshtian, G. Sherbaf, S. Sahraian, and H. I. Sair, "Functional connectivity in neurodegenerative disorders: Alzheimer's disease and frontotemporal dementia," *Topics Magn. Reson. Imag.*, vol. 28, no. 6, pp. 317–324, Dec. 2019.
- [6] N. Tzourio-Mazoyer *et al.*, "Automated anatomical labeling of activations in SPM using a macroscopic anatomical parcellation of the MNI MRI single-subject brain," *NeuroImage*, vol. 15, no. 1, pp. 273–289, 2002.
- [7] K. Szewczyk-Krolikowski *et al.*, "Functional connectivity in the basal ganglia network differentiates PD patients from controls," *Neurology*, vol. 83, no. 3, pp. 208–214, Jul. 2014.
- [8] M. Gorges, H.-P. Müller, D. Lulé, A. C. Ludolph, E. H. Pinkhardt, and J. Kassubek, "Functional connectivity within the default mode network is associated with saccadic accuracy in Parkinson's disease: A resting-state fMRI and videooculographic study," *Brain Connectivity*, vol. 3, no. 3, pp. 265–272, Jun. 2013.
- [9] X. Chen *et al.*, "High-order resting-state functional connectivity network for MCI classification," *Hum. Brain Mapping*, vol. 37, no. 9, pp. 3282–3296, 2016.
- [10] B. Ibrahim *et al.*, "Diagnostic power of resting-state fMRI for detection of network connectivity in Alzheimer's disease and mild cognitive impairment: A systematic review," *Hum. Brain Mapping*, vol. 42, no. 9, pp. 2941–2968, May 2021.
- [11] A. Ortiz, J. Munilla, I. Álvarez-Illán, J. M. Górriz, and J. Ramírez, "Exploratory graphical models of functional and structural connectivity patterns for Alzheimer's disease diagnosis," *Frontiers Comput. Neurosci.*, vol. 9, p. 132, Nov. 2015.
- [12] J. G. Lee *et al.*, "Deep learning in medical imaging: General overview," *Korean J. Radiol.*, vol. 18, no. 4, pp. 570–584, 2017.
- [13] L. Zhang, M. Wang, M. Liu, and D. Zhang, "A survey on deep learning for neuroimaging-based brain disorder analysis," *Frontiers Neurosci.*, vol. 14, p. 779, Oct. 2020.
- [14] S.-H. Wang, Q. Zhou, M. Yang, and Y.-D. Zhang, "ADVIAN: Alzheimer's disease VGG-inspired attention network based on convolutional block attention module and multiple way data augmentation," *Frontiers Aging Neurosci.*, vol. 13, Jun. 2021, Art. no. 687456.
- [15] H. Li *et al.*, "A deep learning model for early prediction of Alzheimer's disease dementia based on hippocampal magnetic resonance imaging data," *Alzheimer's Dementia*, vol. 15, no. 8, pp. 1059–1070, Aug. 2019.
- [16] S. Wang *et al.*, "Single slice based detection for Alzheimer's disease via wavelet entropy and multilayer perceptron trained by biogeography-based optimization," *Multimedia Tools Appl.*, vol. 77, no. 9, pp. 10393–10417, May 2018.
- [17] Y. Cui *et al.*, "Identifying brain networks at multiple time scales via deep recurrent neural network," *IEEE J. Biomed. Health Informat.*, vol. 23, no. 6, pp. 2515–2525, Nov. 2019.
- [18] Q. Dong *et al.*, "Modeling hierarchical brain networks via volumetric sparse deep belief network," *IEEE Trans. Biomed. Eng.*, vol. 67, no. 6, pp. 1739–1748, Jun. 2020.
- [19] C. Baur, S. Denner, B. Wiestler, N. Navab, and S. Albarqouni, "Autoencoders for unsupervised anomaly segmentation in brain MR images: A comparative study," *Med. Image Anal.*, vol. 69, Apr. 2021, Art. no. 101952.
- [20] Z. Zhao, B. Li, R. Dong, and P. Zhao, "A surface defect detection method based on positive samples," in *Proc. PRICAI*, vol. 11013, 2018, pp. 473–481.
- [21] I. Brocas and J. D. Carillo, "The brain as a hierarchical organization," *Amer. Econ. Rev.*, vol. 98, no. 4, pp. 1312–1346, Sep. 2008.
- [22] S. Whitfield-Gabrieli and A. Nieto-Castanon, "Conn: A functional connectivity toolbox for correlated and anticorrelated brain networks," *Brain Connectivity*, vol. 2, no. 3, pp. 125–141, Jun. 2012.
- [23] R. D. Hjelm, V. D. Calhoun, R. Salakhutdinov, E. A. Allen, T. Adali, and S. M. Plis, "Restricted Boltzmann machines for neuroimaging: An application in identifying intrinsic networks," *Neuroimage*, vol. 96, no. 8, pp. 245–260, 2014.
- [24] D. Kuang, X. Guo, X. An, Y. Zhao, and L. He, "Discrimination of ADHD based on fMRI data with deep belief network," in *Proc. Int. Conf. Intell. Comput.*, 2014, pp. 225–232.
- [25] K. H. Cho, T. Raiko, and A. Ilin, "Gaussian-Bernoulli deep Boltzmann machine," in *Proc. Int. Joint Conf. Neural Netw. (IJCNN)*, Aug. 2013, pp. 1–7.
- [26] G. E. Hinton, S. Osindero, and Y.-W. Teh, "A fast learning algorithm for deep belief nets," *Neural Comput.*, vol. 18, no. 7, pp. 1527–1554, 2006.
- [27] X. Hu *et al.*, "Latent source mining in FMRI via restricted Boltzmann machine," *Hum. Brain Mapping*, vol. 39, no. 6, pp. 2368–2380, Jun. 2018.
- [28] H. Huang *et al.*, "Modeling task fMRI data via deep convolutional autoencoder," *IEEE Trans. Med. Imag.*, vol. 37, no. 7, pp. 1551–1561, Jul. 2018.
- [29] V. J. Schmithorst and S. K. Holland, "Comparison of three methods for generating group statistical inferences from independent component analysis of functional magnetic resonance imaging data," *J. Magn. Reson. Imag.*, vol. 19, no. 3, pp. 365–368, Mar. 2004.
- [30] W. Zhang *et al.*, "Hierarchical organization of functional brain networks revealed by hybrid spatiotemporal deep learning," *Brain Connectivity*, vol. 10, no. 2, pp. 72–82, Mar. 2020.
- [31] C. Cortes and V. Vapnik, "Support-vector networks," *Mach. Learn.*, vol. 20, no. 3, pp. 273–297, 1995.
- [32] N. Masuda, M. Sakaki, T. Ezaki, and T. Watanabe, "Clustering coefficients for correlation networks," *Frontiers Neuroinform.*, vol. 12, p. 7, Mar. 2018.
- [33] M. Ota *et al.*, "Structural brain network correlated with reading impairment in Alzheimer's disease," *Dementia Geriatric Cogn. Disorders*, vol. 49, no. 3, pp. 264–269, 2020.
- [34] S. Huang *et al.*, "Whole-brain functional network disruption in chronic pain with disk herniation," *Pain*, vol. 160, no. 12, pp. 2829–2840, Dec. 2019.
- [35] C. Echávarri *et al.*, "Atrophy in the parahippocampal gyrus as an early biomarker of Alzheimer's disease," *Brain Struct. Function*, vol. 215, nos. 3–4, pp. 265–271, 2011.
- [36] J. Tobias Springenberg, A. Dosovitskiy, T. Brox, and M. Riedmiller, "Striving for simplicity: The all convolutional net," 2014, *arXiv:1412.6806*. [Online]. Available: <http://arxiv.org/abs/1412.6806>
- [37] C. Olah, A. Mordvintsev, and L. Schubert, "Feature visualization," *Distill*, vol. 2, no. 11, p. e7, 2017.
- [38] R. R. Selvaraju, M. Cogswell, A. Das, R. Vedantam, D. Parikh, and D. Batra, "Grad-CAM: Visual explanations from deep networks via gradient-based localization," in *Proc. IEEE Int. Conf. Comput. Vis. (ICCV)*, Oct. 2017, pp. 618–626.
- [39] M. E. Raichle, A. M. MacLeod, A. Z. Snyder, W. J. Powers, D. A. Gusnard, and G. L. Shulman, "A default mode of brain function," *Proc. Nat. Acad. Sci. USA*, vol. 98, no. 2, pp. 676–682, 2001.
- [40] L. Qiao, H. Zhang, M. Kim, S. Teng, L. Zhang, and D. Shen, "Estimating functional brain networks by incorporating a modularity prior," *NeuroImage*, vol. 141, pp. 399–407, Nov. 2016.